Review of Scientific Instruments ARTICLE pubs.aip.org/aip/rsi

Spin alignment based Rb-87 magnetometry with free spin precession

Cite as: Rev. Sci. Instrum. 96, 033102 (2025); doi: 10.1063/5.0242881
Submitted: 8 October 2024 • Accepted: 4 March 2025 •
Published Online: 26 March 2025

View Online Export Citation CrossMark

Yang Li,[1] Lulu Zhang,[1] Yongbiao Yang,[1] Junye Zhao,[1] Yanhua Wang,[2,3] Baodong Yang,[2,3] and Junmin Wang[1,3,a)]

AFFILIATIONS

[1] State Key Laboratory of Quantum Optics Technologies and Devices, and Institute of Opto-Electronics, Shanxi University, Taiyuan 030006, China
[2] School of Physics and Electronic Engineering, Shanxi University, Taiyuan 030006, China
[3] Collaborative Innovation Center of Extreme Optics, Shanxi University, Taiyuan 030006, China

[a)] **Author to whom correspondence should be addressed:** wwjjmm@sxu.edu.cn

ABSTRACT

Spin alignment based Rb-87 magnetometry with free spin precession has been proposed. A 795-nm linearly polarized laser beam, serving as the pump beam and the probe beam, propagates through a cylindrical Rb-87 enriched atomic vapor cell along the Z axis, with the polarization orientation aligned along the Y axis. Simultaneously, the static magnetic field $\vec{B_0}$ is applied along the Y axis, and the $\pi/2$ pulse radio-frequency (RF) magnetic field $\vec{B_{RF}}$ is applied along the Z axis. Given that the laser polarization direction aligns with the static magnetic field, the pump beam exhibits π polarization. This induces a symmetric population distribution of ground-state atoms across the Zeeman sublevels. This leads to the generation of a magnetic quadrupole moment, thereby facilitating the formation of the spin alignment state. The $\pi/2$ pulse RF magnetic field aligns the magnetic quadrupole moment with the direction of the RF magnetic field. Upon the cessation of the RF magnetic field, the magnetic quadrupole moment undergoes precession around the static magnetic field. The linearly polarized probe beam, in conjunction with a balanced polarimeter comprising a true zero-order half-wave plate, a Wollaston prism, and a balanced differential photodiode, is employed to measure the free precession decay signal. In this magnetometry system, both the pump power and the RF magnetic field strength have been optimized. The sensitivity of the spin alignment based Rb-87 magnetometry with free spin precession is about 1.7 pT/Hz$^{1/2}$.

I. INTRODUCTION

With the advancement of science and technology, high-sensitivity magnetic field measurement techniques have undergone significant development. Atomic magnetometry, grounded in quantum theory, has emerged as a significant technique. With the continuous advancements in laser technology, the sensitivity of atomic magnetometry continues to improve. Currently, the primary types of high-sensitivity magnetometry include nuclear precession magnetometry, optical pump atomic magnetometry,[1,2] and superconducting quantum interference magnetometry.[3] Owing to its high sensitivity, rapid response, and broad measurement range, superconducting quantum interference magnetometry is widely applied in fields such as brain magnetic measurement, nuclear magnetic resonance, and non-destructive testing.[4–7] However, due to the substantial temperature control apparatus required, the application range of superconducting quantum interference device magnetometry is significantly limited.

Optically pumped atomic magnetometry[8–13] has undergone significant development, primarily due to its advantages in miniaturization and high sensitivity. In 2010, the sensitivity of the spin-exchange relaxation free (SERF) magnetometry[5] reached 0.16 fT/Hz$^{1/2}$. Depending on the polarization of the pump beam, optical pump magnetometry can be categorized into spin-orientation magnetometry and spin-alignment magnetometry.[14,15] In 2007, Budker's research group introduced a spin alignment optical pump atomic magnetometry technique based on the nonlinear magneto-optical rotation effect, known as nonlinear magneto-optical rotation (NMOR) magnetometry.[16] Atoms are polarized by a linearly polarized beam, with a static magnetic field applied along the polarization direction and a small-amplitude alternating magnetic field introduced along the beam propagation direction to detect the alternating magnetic field. The calibrated sensitivity of this magnetometry system is 10 fT/Hz$^{1/2}$. In 2024, S. Zou's research group enhanced this magnetometry by replacing the small-amplitude alternating magnetic field with a $\pi/2$ pulse radio-frequency (RF) magnetic field,[17] introducing a repump beam, and detecting the free spin precession decay signal to measure the static magnetic field. Ultimately, the sensitivity is measured at 0.16 pT/Hz$^{1/2}$ under zero magnetic field. To enhance the practicality and simplicity of optical pump atomic magnetometry, a single-beam-based optical pump atomic magnetometry system is proposed in this paper.

In this study, a spin alignment based Rb-87 magnetometry with free spin precession has been proposed, driven by the π-polarized beam and the $\pi/2$ pulse RF magnetic field. The parameters for the pump beam intensity and RF magnetic field strength in the magnetometry system are optimized through the observation of the magnetic resonance signal, followed by the calculation of the system's sensitivity. The magnetometry employs a single-beam design, where the plane of linear polarization is rotated due to the circular dichroism of the light. It operates based on the same principle as NMOR magnetometry.

II. THEORETICAL ANALYSIS

The underlying principle of optically pumped atomic magnetometry is based on the interaction between an atomic ensemble and both magnetic and light fields. It determines the magnitude of the measured magnetic field by measuring the Larmor precession frequency of the atomic spin polarization vector in the external magnetic field.[18] Alkali metal atoms, such as Rb and Cs, are commonly used as the medium for interaction with light fields in optically pumped atomic magnetometry. When atoms absorb photons, the ground state atoms transition to the excited state, subsequently returning to the ground state via spontaneous decay. Continuous photon pumping causes the atoms to transition back to the excited state, eventually undergoing spontaneous decay to the ground state, which does not interact with photons (the dark state), thus completing the optical pumping process.[19] When an RF magnetic field is applied, a magnetic dipole transition occurs between adjacent Zeeman energy levels. When the frequency of the RF magnetic field matches the precession frequency of the atomic magnetic moment in the external magnetic field, known as the Larmor precession frequency, the magnetic dipole transition rate reaches its maximum. However, different types of optically pumped atomic magnetometry employ distinct detection methods to observe the dynamic evolution of the atomic behavior.[20] For example, Mz type optically pumped atomic magnetometry utilizes magnetic dipole transitions induced by an alternating magnetic field to depolarize the atomic ensemble. Subsequently, the transmitted beam intensity is reduced due to reabsorption by the atoms, which is then used to measure the magnetic field.[21] Spin alignment based Rb magnetometry with free spin precession exploits the circular dichroism of light to measure the magnetic field. Circular dichroism occurs when a π polarized beam passes through the vapor cell, causing the beam polarization to rotate due to the differing absorption rates of atoms for σ^+ and σ^- polarized components.[22] The measurement principle follows the same approach as NMOR magnetometry.

A. Preparation of spin alignment of Rb-87 atoms

The initial step in measuring a magnetic field using optically pumped atomic magnetometry is to polarize the atoms. The atomic polarization state is defined as follows: when all atoms in an ensemble occupy the same quantum state, the entire ensemble can be described by a collective wave function, and the atoms are considered to be in a polarized state. In the magnetometry system, optical pumping technology is employed to achieve the polarization of the atomic ensemble. The various polarization states of the pumped beam induce the polarization of the atomic ensemble into corresponding states. The 795-nm π-polarized pump beam, resonating with the D1 line $(F_g = 2) \to (F_e = 1)$ transition of the Rb-87 atom, excites the atom from the ground state to the excited state, after which the excited atom relaxes to the various Zeeman sublevels of the ground state via spontaneous decay. Continuous excitation by the π-polarized pump beam causes most atoms to eventually populate the $m_F = -2$ and $m_F = +2$ Zeeman levels of the ground state. At this point, some atoms remain in other Zeeman levels of the ground state, thus completing the preparation of the spin alignment for Rb-87 atoms. Figure 1 presents the physical depiction of spin alignment based Rb-87 magnetometry with free spin precession.

B. Simplified atomic spin evolution model

Model construction for transitions of ground state angular momentum $F_g > 1$ is complex. Therefore, for simplicity, a reduced model of the $(F_g = 1) - (F_e = 0)$ transition is considered to obtain the analytical solution. We describe the density matrix form analysis in the experimental process. The time evolution of the density matrix $\hat{\rho}$ is given by the Liouville equation

$$\frac{d\hat{\rho}}{dt} = -i[\hat{H}, \hat{\rho}] - \frac{1}{2}\{\hat{\xi}, \hat{\rho}\} + \hat{\Lambda}, \tag{1}$$

where $\hat{H}$ is the total Hamiltonian of the system, $\hat{\xi}$ is the relaxation operator, and $\hat{\Lambda}$ is the repopulation operator

$$\hat{H} = \begin{pmatrix} \Omega_L & \frac{\Omega_{RF}\cos(\omega_{RF}t)}{\sqrt{2}} & 0 & 0 \\ \frac{\Omega_{RF}\cos(\omega_{RF}t)}{\sqrt{2}} & 0 & \frac{\Omega_{RF}\cos(\omega_{RF}t)}{\sqrt{2}} & -\frac{\Omega_R\cos(\omega t)}{\sqrt{3}} \\ 0 & \frac{\Omega_{RF}\cos(\omega_{RF}t)}{\sqrt{2}} & -\Omega_L & 0 \\ 0 & -\frac{\Omega_R\cos(\omega t)}{\sqrt{3}} & 0 & \omega_0 \end{pmatrix}. \tag{2}$$

Here, $\Omega_L = \gamma_g B_0$ represents the Larmor precession frequency corresponding to the static magnetic field $\vec{B_0}$, where γ_g denotes the gyromagnetic ratio for the $F_g = 1$ state. $\Omega_{RF} = g_F \mu_B B_{RF}/\hbar$ is the magnetic Rabi frequency associated with the RF magnetic field $\vec{B_{RF}}$, where g_F is the Landé g-factor for the $F_g = 1$ state, and μ_B represents the Bohr magneton. Ω_R represents the Rabi frequency for the optical transition induced by the probe beam, ω denotes the frequency of the probe beam, ω_{RF} refers to the frequency of the RF magnetic field, and ω_0 is the resonance frequency for the $(F_g = 1) - (F_e = 0)$

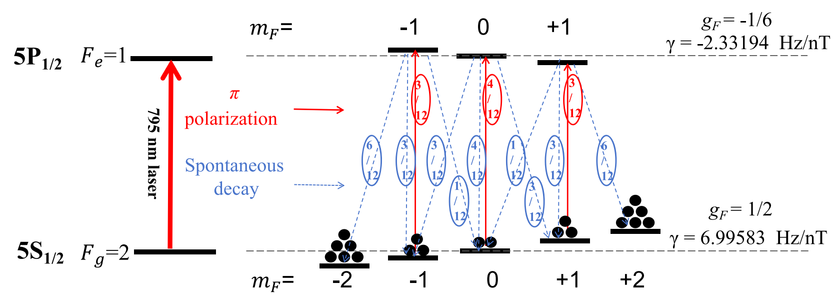

FIG. 1. Atomic spin alignment of Rb-87 atoms prepared by a 795-nm linearly polarized (π polarization) laser beam. The numbers within the ellipse indicate the relative probabilities of the transitions.

transition. In the case where the RF magnetic field is disabled during detection, the system's Hamiltonian can be simplified as[17]

$$\hat{H}' = \begin{pmatrix} \Omega_L & 0 & 0 & 0 \\ 0 & 0 & 0 & -\dfrac{\Omega_R}{2\sqrt{3}} \\ 0 & 0 & -\Omega_L & 0 \\ 0 & -\dfrac{\Omega_R}{2\sqrt{3}} & 0 & 0 \end{pmatrix}. \tag{3}$$

The relaxation rate of the system can be given by the following matrix:

$$\hat{\xi} = \begin{pmatrix} \gamma & 0 & 0 & 0 \\ 0 & \gamma & 0 & 0 \\ 0 & 0 & \gamma & 0 \\ 0 & 0 & 0 & \Gamma + \gamma \end{pmatrix}. \tag{4}$$

Here, γ is the uniform relaxation rate of the ground state and excited state, and its related factors include the wall collisions, buffer gas collisions, diffusion of atoms from the beam area, or unpolarized atoms flowing from the vapor cell stem. Γ is the relaxation rate of the excited state, mainly due to the spontaneous decay of the excited state atoms. The matrix $\hat{\Lambda}$ describes the repopulation of the number of atoms in the ground state due to the spontaneous decay of atoms in the excited state and is represented by the following matrix:

$$\hat{\Lambda} = \begin{pmatrix} \dfrac{\gamma + \Gamma\rho_{e_0e_0}}{3} & 0 & 0 & 0 \\ 0 & \dfrac{\gamma + \Gamma\rho_{e_0e_0}}{3} & 0 & 0 \\ 0 & 0 & \dfrac{\gamma + \Gamma\rho_{e_0e_0}}{3} & 0 \\ 0 & 0 & 0 & 0 \end{pmatrix}. \tag{5}$$

The time evolution of the elements in the density matrix is determined by the Liouville equation, as shown below:

$$\frac{d\rho_{g_{\pm1}e_0}}{dt} = -\left(\frac{\Gamma}{2} + \gamma \pm i\Omega_L\right)\rho_{g_{\pm1}e_0} - \frac{i\Omega_R\rho_{g_{\pm1}g_0}}{2\sqrt{3}}, \tag{6}$$

$$\frac{d\rho_{g_{\pm1}g_0}}{dt} = -\frac{i\Omega_R\rho_{g_{\pm}e_0}}{2\sqrt{3}} - (\gamma \pm i\Omega_L)\rho_{g_{\pm1}g_0}. \tag{7}$$

The subscript of $\rho_{g_{\pm1}e_0}$ in the above-mentioned formula represents the Zeeman sub-level, which can be expressed as the particle population change caused by the relaxation rate of the excited state is significantly greater than that caused by other factors, $\rho_{g_{\pm1}e_0}$ can be represented by Eq. (8), where a and b are real numbers,

$$\rho_{g_{\pm1}e_0} = \frac{(-ai + b)e^{t(-\gamma \mp i\Omega_L)}\Omega_R}{\sqrt{3}\Gamma}. \tag{8}$$

From the expectation value of the polarization of the medium, the optical-rotation signal per unit length dl of the medium can be written in the form of the following equation:[23]

$$\frac{d\theta}{dt} = \frac{\sqrt{3}n_d\Gamma\lambda^2}{2\sqrt{2\pi}\Omega_R}\,\mathrm{Im}\left(\rho_{g_{-1}e_0} - \rho_{g_1e_0}\right), \tag{9}$$

where λ refers to the wavelength of the probe beam and n_d is the atomic density. Combined with the above-mentioned equation, the magnitude of the optical rotation signal can be expressed as

$$\frac{d\theta}{dt} = \frac{bn_d\lambda^2}{2\sqrt{2\pi}}e^{-t\gamma_{\gamma f}}\,\sin(\Omega_L t). \tag{10}$$

Equation (10) shows that the signal is an exponentially decayed sine wave whose frequency corresponds to the Larmor precession frequency.

III. EXPERIMENTAL SETUP

As shown in Fig. 2, the spin alignment based Rb-87 magnetometry with free spin precession is implemented experimentally. The experiment employs a cylindrical Rb-87 enriched atomic vapor cell with a paraffin coating on its inner wall. The Rb atomic vapor cell has a diameter of 25 mm and a length of 75 mm. The Rb atomic vapor cell is positioned within a cylindrical four-layer Permalloy magnetic shielding barrel, with a typical shielding factor exceeding 10 000. A 795-nm π-polarized pump laser beam (also serving as the probe beam), with its polarization direction along the Y axis, propagates along the Z axis through the Rb atomic vapor cell at room temperature. The pump beam, with a waist radius of ~10 mm, is tuned to the Rb-87 D1 line $Fg = 2$ to $F_e = 1$ transition using the polarization spectroscopic device. Meanwhile, three pairs of Helmholtz magnetic coils, driven by low-noise DC or AC currents along the X, Y, and Z axes, generate the static magnetic field $\vec{B_0}$ along the Y axis and the $\pi/2$ pulse RF magnetic field $\vec{B_{RF}}$ along the Z axis. The frequency of the RF magnetic field is resonant with the Larmor precession frequency. The balanced differential photodiode data, representing the free spin precession decay signal, are acquired using a data acquisition card (NI USB-6363).

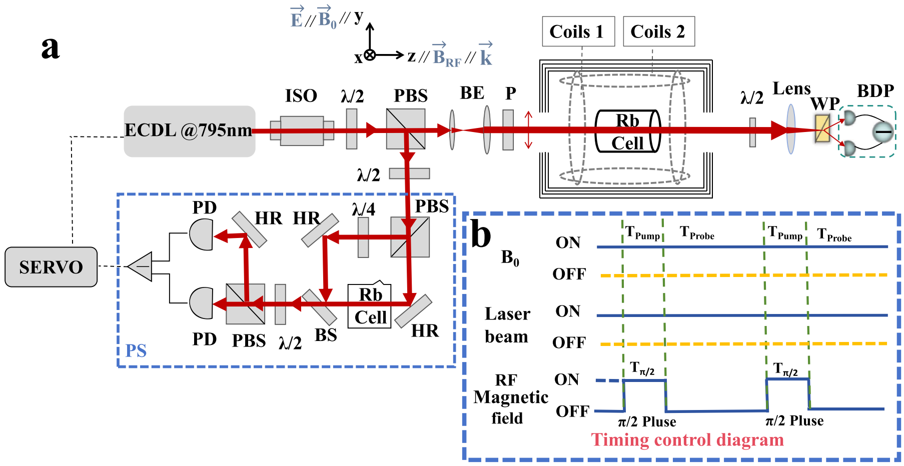

FIG. 2. (a) Schematic diagram of experimental setup and timing control diagram of the spin alignment based Rb-87 magnetometry with free spin precession. ECDL: external-cavity diode laser; ISO: optical isolator; $\lambda/2$: half-wave plate; PBS: polarization beam splitter; BE: the beam expanding telescope; P: polarizer; Coils 1, Coils 2: Helmholtz coils; WP: Wollaston prism; BDP: balanced differential photodiodes; $\lambda/4$: quarter-wave plate; HR: high-reflectivity mirror; BS: beam splitter mirror; PD: photodetector; PS: the polarization spectroscopic device. (b) Timing control diagram.

The magnetic resonance signal is then obtained via fast Fourier transform.

The frequency of the RF magnetic field is maintained in resonance with the Larmor precession frequency, and the RF magnetic field is periodically controlled. Initially, the π-polarized beam passes through the atomic vapor cell to polarize the atoms. A $\pi/2$ pulse RF magnetic resonance causes the magnetic quadrupole moment to gradually precess in the direction of the RF magnetic field. The theoretical duration of the $\pi/2$ pulse RF magnetic resonance can be calculated using Eq. (11). During the experimental procedure, the duration of the $\pi/2$ pulse RF magnetic resonance is determined through monitoring the magnetometry signal. As the RF magnetic field is applied, the magnetometry signal increases, and upon reaching its maximum, the duration of the corresponding RF magnetic field is identified as the $\pi/2$ pulse RF magnetic resonance,

$$t_{\pi/2} = \frac{\pi}{2\Omega_{RF}}. \tag{11}$$

Once the RF magnetic field is turned off, the atoms will be re-polarized, and the magnetic quadrupole moment will precess around the direction of the static magnetic field. Due to the circular dichroism of the light, when the π-polarized beam passes through the atomic vapor cell, the σ^+ and σ^- polarized components of the π-polarized beam are absorbed differently, causing the polarization plane of the light field to rotate. At this point, the linearly polarized probe beam, in conjunction with a balanced polarimeter comprising a true zero-order half-wave plate, a Wollaston prism, and a balanced differential photodiode, is employed to measure the free precession decay signal. The time-domain signal is transformed to the frequency-domain signal using fast Fourier transform, and the Larmor precessional frequency can be extracted through Lorentz line fitting.[24,25]

IV. EXPERIMENTAL RESULTS AND DISCUSSIONS

The experiment achieves spin alignment based Rb-87 magnetometry with free spin precession through periodic control of the RF magnetic field. During each period, when the RF magnetic field is turned off, the free spin precession signal is transformed using fast Fourier transform to obtain the magnetic resonance signal.

According to the basic principle of optical pumping magnetometry,[21] we can perform a fast Fourier transform on the obtained free spin precession signal to obtain the magnetometry resonance signal. By fitting the magnetic resonance signal with a Lorentzian curve, the peak of the fitted curve corresponds to the magnetic field frequency at which the magnetic dipole transition rate is maximized. When the RF magnetic field frequency is equal to the system's Larmor precession frequency, the magnetic dipole transition rate reaches its maximum. Therefore, the magnetic field frequency at the peak of the fitted curve corresponds to the Larmor precession frequency. When the RF magnetic field frequency is detuned from the Larmor precession frequency, the magnetic dipole transition rate decreases, leading to a reduction in the magnetometer signal. The Larmor precession frequency is extracted via Lorentz line fitting of the magnetic resonance signal. The transverse relaxation time (T_2) of the atomic ensemble is determined by fitting the free spin precession decay signal. Figures 3 and 4 show the magnetometry signal diagram and the magnetic resonance signal diagram, respectively.

Based on the deduction from Eq. (10), the decaying signal of free spin precession in Fig. 3 is an exponentially decaying positive wave with a frequency corresponding to the Larmor precession. Meanwhile, the magnetic resonance signal in Fig. 4 exhibits a resonance frequency that matches the Larmor precession frequency, which is in agreement with theoretical expectations. The relationship between T_2 and the HWHM of the magnetic resonance signal is

$$T_2 \propto \frac{1}{\Delta \upsilon}, \tag{12}$$

where T_2 represents the transverse relaxation time, while $\Delta\upsilon$ denotes the HWHM of the magnetic resonance signal. In addition, T_2 is inversely proportional to $\Delta\upsilon$.

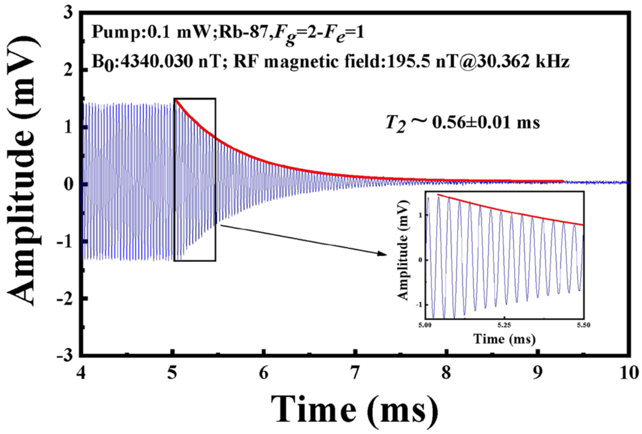

FIG. 3. Typical free spin precession signal of the spin alignment based Rb-87 magnetometry after the $\pi/2$ pulse RF magnetic field. The spin transverse relaxation time of the Rb-87 spin alignment state, T_2, is about 0.56 ms obtained by exponential decay fitting. The inset is a zooming view of the partial signal of free spin precession.

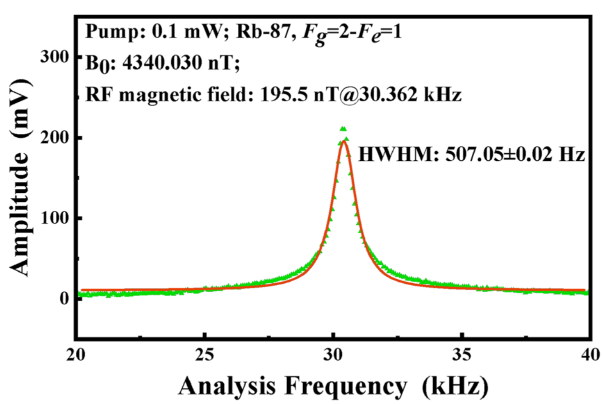

FIG. 4. Magnetic resonance signal is achieved by FFT of the free spin precession signal of the Rb-87 spin alignment (the green dots). The red curve is Lorentzian fitting. The typical half-width half-maximum (HWHM) linewidth of the magnetic resonance signal is about 507.05 Hz.

A. Parameter optimization

Within a specified range, an increase in the intensity of the RF magnetic field enhances the rate of magnetic dipole transitions between the Zeeman sublevels. However, this increase is accompanied by a rise in noise. Similarly, while an increase in pump power improves the polarization of the atomic system, it simultaneously introduces additional noise. Consequently, determining the optimal RF magnetic field strength and pump power is crucial for enhancing the sensitivity of the atomic magnetometry. After obtaining the magnetic resonance signal, the RF magnetic field strength and the intensity of the polarized beam in the magnetometry system are varied. The amplitude of the magnetic resonance signal, its HWHM, and amplitude/HWHM are monitored as the variables are adjusted.

Figures 5 and 6 illustrate the variations in the amplitude, HWHM, and amplitude/HWHM of the magnetic resonance signal as a function of changes in the RF magnetic field and pump power, respectively. As shown in Fig. 5(a), owing to the RF field being switched off during the decay process of free spin precession, the HWHM of the magnetic resonance signal remains largely unaffected by the noise induced by the increasing RF magnetic field. Figures 5(b) and 5(c) indicate that as the RF magnetic field strength increases, the amplitude and amplitude/HWHM of the magnetic resonance signal increase within a certain range and then stabilize. This is due to the fact that, as the RF magnetic field strength increases, the magnetic dipole transition rate rises within a specific range before eventually reaching saturation. As shown in Figs. 6(a)–6(c), within a specific range, as the intensity of the polarized beam increases, the HWHM, amplitude, and amplitude/HWHM of the magnetic resonance signal correspondingly increase. This can be attributed to the fact that, within this range, the light pumping rate increases concomitantly with the intensity of the polarized beam, while the noise also escalates. Given that the sensitivity of the magnetometry is related to the narrow linewidth and amplitude of the magnetic resonance signal, it is determined by selecting the appropriate parameters from the figures mentioned earlier.

B. Experimental results

Based on the amplitude and HWHM of the processed magnetic resonance signal, the RF magnetic field strength is set to 195.5 nT, and the pump beam power is adjusted to 0.1 mW. The duration of the $\pi/2$ RF magnetic field is determined to be ~1.15 ms, as calculated from Eq. (11). The duration of the $\pi/2$ RF magnetic field is coincident with the duration of the pump beam. Subsequently, spin alignment based Rb-87 magnetometry with free spin precession signals over multiple periods is recorded using a LabVIEW program. A Power Spectral Density (PSD) program is written in MATLAB to calculate the static magnetic field measurement values and magnetometry sensitivity and to calibrate both the sensitivity and static magnetic field measurement values using statistical averaging. The research group led by S. Zou proposed Rb atomic magnetometry based on spin alignment states,[26] where an alternating magnetic field is continuously applied. The system uses a lock-in amplifier to demodulate the weak signals from the balanced differential detection and utilizes low-frequency alternating fields for sensitivity calibration. In contrast, the Rb-87 atomic magnetometry based on spin alignment states proposed in this paper operates with the alternating magnetic field turned off during the detection phase. The static magnetic field is directly calculated from the balanced differential detection signal using a fast Fourier transform, and the magnetometry sensitivity is obtained by computing the PSD of the magnetic field noise from 8000 static magnetic field measurement values. This approach offers a significant simplification in the system's complexity.

The magnetic field measurement value B_0 of 4340.027 nT is obtained by performing Gaussian fitting on the frequency distribution shown in Fig. 7 and carrying out statistical averaging. Figure 8 illustrates the PSD of the magnetic field noise within the analysis frequency range of 0–25 Hz. Given that the PSD of the magnetic field noise in the 0–1 Hz range is relatively large and does not meet the

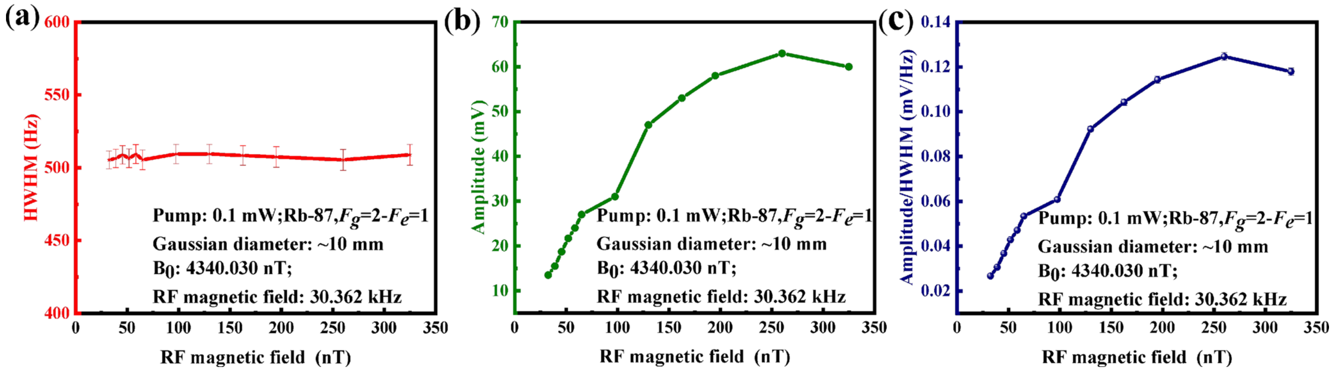

FIG. 5. (a) HWHM vs RF magnetic field strength, (b) amplitude vs RF magnetic field strength, and (c) amplitude/HWHM vs RF magnetic field strength.

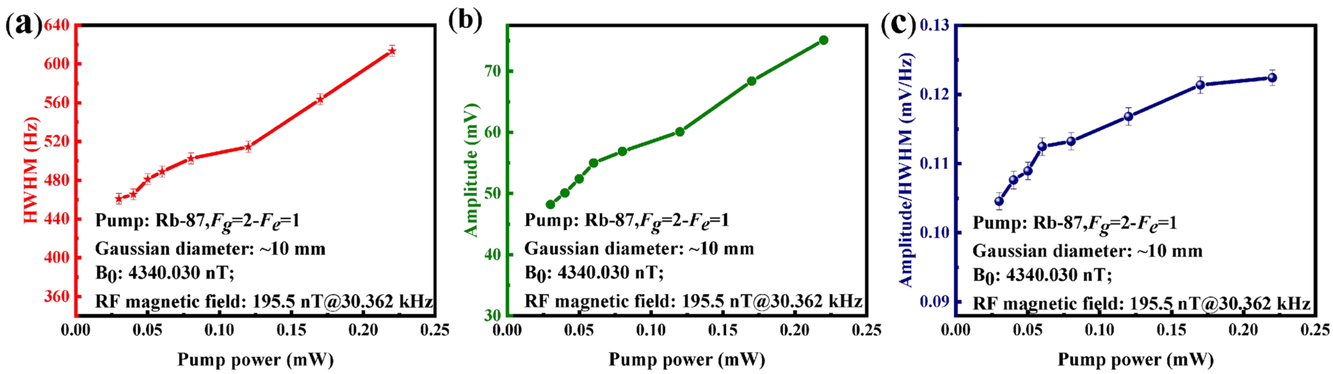

FIG. 6. (a) HWHM vs pump power, (b) amplitude vs pump power, and (c) amplitude/HWHM vs pump power.

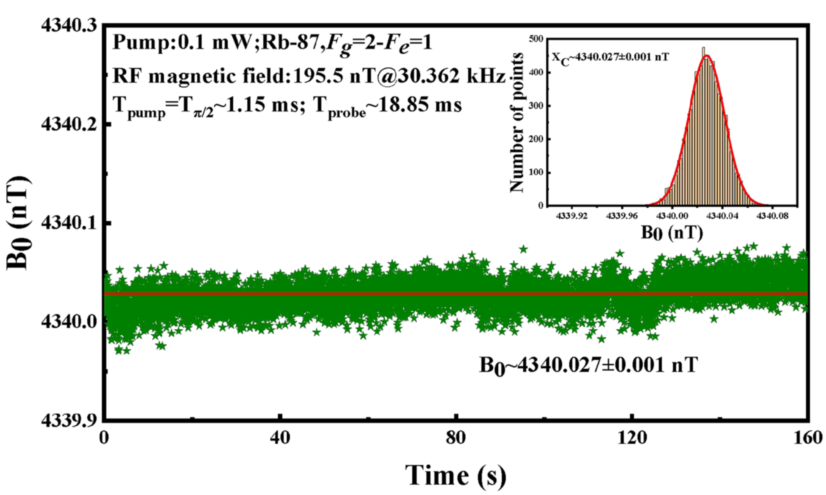

FIG. 7. 8000 green asterisk markers represent the static magnetic field measurement values. Each value is derived from a free spin precession signal with a period of 20 ms. The red line represents the static magnetic field measurement value after statistical averaging. The typical static magnetic field measurement value is ~4340.027 nT. The static magnetic field value expected to be output by the coil is 4340.030 nT. The inset illustrates the typical static magnetic field measurement values obtained through statistical averaging and Gaussian fitting of the static magnetic field values over 8000 periods.

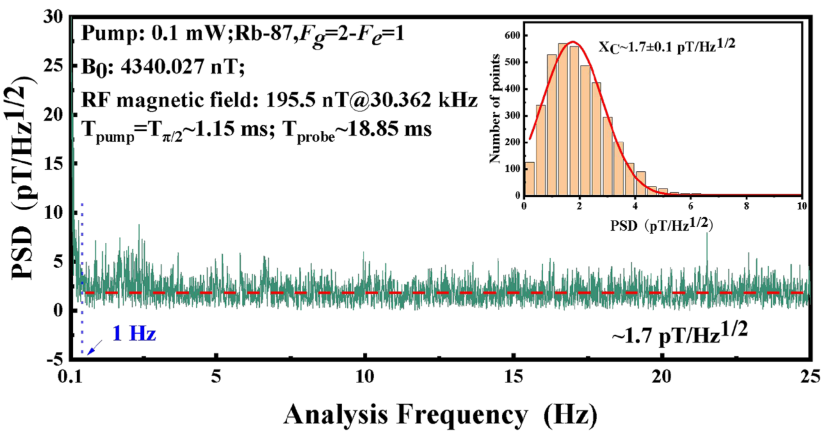

FIG. 8. Green curve represents the PSD of static magnetic field noise calculated from 8000 static magnetic field measurement values, while the red dashed line indicates the magnetometry sensitivity derived from the statistical averaging of the PSD over the analysis frequency range of 1–25 Hz. The typical magnetometry sensitivity is ~1.7 pT/Hz$^{1/2}$. The inset illustrates the magnetometry sensitivity obtained after statistical averaging and Gaussian fitting of the PSD of static magnetic field noise within the analysis frequency range of 1–25 Hz.

statistical criteria, the frequency distribution and Gaussian fitting of the PSD are performed over the 1–25 Hz range. The sensitivity of the spin alignment based Rb-87 magnetometry with free spin precession is 1.7 pT/Hz$^{1/2}$.

V. CONCLUSIONS

In conclusion, a spin alignment based Rb-87 atomic magnetometry with free spin precession has been successfully implemented and characterized experimentally. A single 795-nm π-polarized laser beam, which serves both as the pump and probe beam, is passed through a paraffin-coated Rb-87 enriched vapor cell. The Rb vapor cell, serving as the sensor element, is positioned within a four-layer permalloy cylindrical magnetic shield, which has a typical shielding factor greater than 10 000. A $\pi/2$ pulse RF magnetic field is applied to the Rb-87 atoms. The pump power and RF magnetic field strength in the magnetometry system are optimized, yielding a sensitivity of 1.7 pT/Hz$^{1/2}$ for the spin alignment based Rb-87 magnetometry with free spin precession.

In subsequent experiments, the linewidth of the magnetic resonance signal can be narrowed by increasing the beam diameter of the polarized beam or enhancing the magnetic field uniformity at the location of the atomic vapor cell. In addition, the intensity noise of the polarized beam within the magnetometry system and the current noise from the magnetic field source can also be optimized.

Compared to absorption-based schemes, the use of a linearly polarized detection beam and balanced detection significantly reduces the impact of common-mode noise and laser intensity fluctuations on the magnetometry sensitivity. In real-world applications, this type of magnetometry significantly optimizes the optical-pumping atomic magnetometry system while maintaining a certain level of sensitivity and measurable range. In addition, because its measurement range can reach the magnitude of the Earth's magnetic field, it is a good choice for measuring environmental magnetic fields. The single beam design and high sensitivity of this magnetometry hold significant potential for simplifying the commercialization of optical pump atomic magnetometry.

ACKNOWLEDGMENTS

This work was supported by the National Natural Science Foundation of China (Grant No. 12474483) and the Fundamental Research Program of Shanxi Province of China (Grant No. 202403021211013).

AUTHOR DECLARATIONS

Conflict of Interest

The authors have no conflicts to disclose.

Author Contributions

Yang Li: Data curation (equal); Formal analysis (equal); Writing – original draft (equal). **Lulu Zhang**: Data curation (equal); Formal analysis (equal); Resources (equal); Software (equal). **Yongbiao Yang**: Formal analysis (equal); Investigation (equal). **Junye Zhao**: Formal analysis (equal); Investigation (equal). **Yanhua Wang**: Investigation (equal). **Baodong Yang**: Investigation (equal); Writing – review & editing (equal). **Junmin Wang**: Conceptualization (lead); Methodology (equal); Project administration (equal); Resources (lead); Supervision (equal); Writing – review & editing (equal).

DATA AVAILABILITY

The data that support the findings of this study are available from the corresponding author upon reasonable request.

REFERENCES

[1] D. Budker and M. Romalis, "Optical magnetometry," Nat. Phys. **3**, 227 (2007).
[2] W. M. Sun, J. H. Zhang, and X. J. Zeng, *Principle and Application of Optical Atomic Magnetometry* (Science Press, 2022) (in Chinese).
[3] J. Clarke, "Principles and applications of SQUIDs," Proc. IEEE **77**, 1208 (1989).
[4] S. H. Ward and K. A. Ruddock, "A field experiment with a rubidium-vapor magnetometer," J. Geophys. Res. **67**, 1889 (1962).
[5] H. B. Dang, A. C. Maloof, and M. V. Romalis, "Ultrahigh sensitivity magnetic field and magnetization measurements with an atomic magnetometer," Appl. Phys. Lett. **97**, 15 (2010).

[6] Y. Hu, G. Z. Iwata, M. Mohammadi, E. V. Silletta, A. Wickenbrock, J. W. Blanchard, D. Budker, and A. Jerschow, "Sensitive magnetometry reveals inhomogeneities in charge storage and weak transient internal currents in li-ion cells," Proc. Natl. Acad. Sci. U. S. A. **117**, 10667 (2020).

[7] R. Zhang, W. Xiao, Y. Ding, Y. Feng, X. Peng, L. Shen, C. Sun, T. Wu, Y. Wu, Y. Yang, Z. Zheng, X. Zhang, J. Chen, and H. Guo, "Recording brain activities in unshielded earth's field with optically pumped atomic magnetometers," Sci. Adv. **6**, 8792 (2020).

[8] F. Zheng, C. Li, D. Li, W. Xu, X. Ru, H. Cheng, Z. Liu, S. Na, L. Qin, B. Lyu, and J. H. Gao, "A compact triaxial SERF magnetometer with high sensitivity and 1.1 kHz bandwidth for magnetoencephalography," IEEE Sens. J. **24**, 28722 (2024).

[9] K. K. Huang, N. Li, and X. H. Lu, "A high sensitivity laser-pumped cesium magnetometer," Chin. Phys. Lett. **29**, 100701 (2012).

[10] W. E. Bell and A. L. Bloom, "Optically driven spin precession," Phys. Rev. Lett. **6**, 280 (1961).

[11] J. C. Allred, R. N. Lyman, T. W. Kornack, and M. V. Romalis, "High-sensitivity atomic magnetometer unaffected by spin-exchange relaxation," Phys. Rev. Lett. **89**, 130801 (2002).

[12] I. K. Kominis, T. W. Kornack, J. C. Allred, and M. V. Romalis, "A subfemtotesla multichannel atomic magnetometer," Nature **422**, 596 (2003).

[13] M. P. Ledbetter, I. M. Savukov, V. M. Acosta, D. Budker, and M. V. Romalis, "Spin-exchange-relaxation-free magnetometry with Cs vapor," Phys. Rev. A **77**, 033408 (2008).

[14] S. Pustelny, A. Wojciechowski, M. Gring, M. Kotyrba, J. Zachorowski, and W. Gawlik, "Magnetometry based on nonlinear magneto-optical rotation with amplitude-modulated light," J. Appl. Phys. **103**, 063108 (2008).

[15] G. Katsoprinakis, D. Petrosyan, and I. K. Kominis, "High frequency atomic magnetometer by use of electromagnetically induced transparency," Phys. Rev. Lett. **97**, 230801 (2006).

[16] M. P. Ledbetter, V. M. Acosta, S. M. Rochester, D. Budker, S. Pustelny, and V. V. Yashchuk, "Detection of radio-frequency magnetic fields using nonlinear magneto-optical rotation," Phys. Rev. A **75**, 023405 (2007).

[17] G. Jin, T. Shi, Y. Zhao, H. Zhang, and S. Zou, "A room-temperature operational alignment magnetometer utilizing free-spin precession," Adv. Quantum Technol. **7**, 2300377 (2024).

[18] H. Haken and H. C. Wolf, *The Physics of Atoms and Quanta: Introduction to Experiments and Theory* (Springer Science, 2006).

[19] M. Auzinsh, D. Budker, and S. Rochester, *Optically Polarized Atoms* (Oxford University Press, 2010).

[20] F. Bloch, "Nuclear induction," Phys. Rev. **70**, 460 (1946).

[21] L. L. Zhang, L. L. Bai, Y. L. Yang, Y. B. Yang, Y. H. Wang, X. Wen, J. He, and J. M. Wang, "Improving the sensitivity of an optically pumped rubidium atomic magnetometer by using of a repumping laser beam," Acta Phys. Sin. **70**, 230702 (2021) (in Chinese).

[22] R. Jiménez-Martínez, W. C. Griffith, S. Knappe, J. Kitching, and M. Prouty, "High-bandwidth optical magnetometer," J. Opt. Soc. Am. B **29**, 3398 (2012).

[23] T. Zigdon, A. D. Wilson-Gordon, S. Guttikonda, E. J. Bahr, O. Neitzke, S. M. Rochester, and D. Budker, "Nonlinear magneto-optical rotation in the presence of a radio-frequency field," Opt. Express **18**, 25494 (2010).

[24] L. M. Rushton, L. Elson, A. Meraki, and K. Jensen, "Alignment-based optically pumped magnetometer using a buffer-gas cell," Phys. Rev. Appl. **19**, 064047 (2023).

[25] D. Budker, D. F. Kimball, S. M. Rochester, and V. V. Yashchuk, "Nonlinear magneto-optical rotation via alignment-to-orientation conversion," Phys. Rev. Lett. **85**, 2088 (2000).

[26] T. Shi, G. Jin, H. Zhang, and S. Zou, "A ^{85}Rb transverse modulation magnetometer in the geophysical range based on atomic alignment states," J. Phys. D: Appl. Phys. **57**, 485002 (2024).